Modeling of Diesel and Diesel-Electric Hybrid Propulsion Systems for Conceptual Design of Rotorcraft

J. Michael Vegh

jmvegh@stanford.edu

PhD Candidate, Aeronautics & Astronautics,

Stanford University

Stanford, CA, 94305, USA

Juan J. Alonso

jjalonso@stanford.edu

Professor, Aeronautics & Astronautics

Stanford University

Stanford, CA, 94305, USA

Jeffrey D. Sinsay

Aerospace Engineer Advanced Design Office,

U.S. Army Research, Development, and Engineering Command, Aviation Development Directorate–AFDD

Moffett Field, CA, USA

ABSTRACT

This paper details the development of a turbocharged diesel model based on a combination of 0D thermodynamic models and fits to publically available diesel engines, taking into account the effect of engine speed and atmospheric effects on engine lapsing characteristics. The model was then extrapolated,and applied to some systems-level trade studies and optimization of diesel as well as diesel-electric tailsitters, which were compared to a reference turboshaft design. Results suggested that, for the mission and architecture of interest, a hybrid-diesel aircraft was able to achieve modest weight and fuel savings over pure diesel designs. On the other hand, optimization revealed numerical issues with satisfying energy and power constraints for the hybrid designs; alternative formulations of the problem may achieve further fuel burn reductions. The turboshaft design, outperformed both the diesel and diesel-electric aircraft for the mission and assumptions shown here, suggesting that alternative configurations and/or improved battery technology are required to properly leverage the benefits of electric propulsion.

INTRODUCTION

Recently, there has been considerable interest in the design of aircraft incorporating electric propulsion technology [1-3]. Nonetheless, present-day battery technology generally prevents the design of all-electric aircraft capable of flying long-range or long-endurance missions. In particular, specific energy is a limiting factor in the design of these aircraft; lithium-ion batteries have a specific energy roughly 1/60th that of conventional fuel sources. For missions and aircraft where the power requirements vary substantially, specific power can also be a limiting factor i.e. the battery may be power, rather than energy limited.

On the other hand, diesel engines are known to offer substantial improvements in specific fuel consumption over turboshaft engines, albeit while suffering significant power-to-weight ratio penalties [4]. For this reason, a number of new vehicle concepts are in development which implement a diesel-electric propulsion system that uses batteries and motors to account for short duration power requirements (e.g. hover), while taking advantage of the high efficiency of diesel engines [5]. Additionally, a given diesel engine (if turbocharged) tends to lapse at a higher altitude than a comparable turboshaft [4]. As a result, aircraft designed using diesel engines, combined with an electric system, will likely not suffer the same off-design operation penalties from “hot and high hover” design requirements. This may offer more flexibility in vehicle operation.

ENGINE CYCLE ANALYSIS

To aid in developing an appropriate model for conceptual design, a 0D cycle-analysis was created to model turbocharged diesel engines with a fixed compression ratio, assuming isentropic compression and expansion, based on the method from Heywood [6]. The compression ratio was 18 and the break altitude for a standard atmosphere was 6000 ft. based on publicly available data from the Centurion 2.0s engine [7]. The cycle is as follows; a compressor acts on the freestream air according to a specific power input, as seen below.

$$T_1 = T_0 + \frac{Spa_{turbocharger}}{cp} \tag{1}$$

$$\frac{p_1}{p_0} = \left(\frac{T_1}{T0}\right)^{\frac{\gamma}{\gamma-1}} \tag{2}$$

$$\rho_1 = \frac{p_1}{RT_1} \tag{3}$$

where $Spa_{turbocharger}$ is the power imparted to the flow normalized by the total mass flow rate through the engine. The compression stroke reduces the volume of the charge of air inside the diesel based on the compression ratio r_c.

$$\rho_2 = \rho_1 * r_c \tag{4}$$

Isentropic compression is assumed, providing both temperature and pressure at the end of the stroke. Then fuel is injected into the chamber, based on an assumed fuel to air ratio of 1/18 at constant pressure, which gives

$$T_3 = T_2 + f * \frac{Q_{lhv}}{cp} \tag{5}$$

where Q_{lhv} is the lower heating value of diesel, and f is the fuel to air ratio. No changes in gas composition properties (such as specific heat) were modeled in this simplified analysis, and a perfect gas was assumed throughout. Furthermore, if T_3 was found to be greater than the adiabatic flame temperature of diesel with air (~2400 K), the adiabatic flame temperature was assumed, and a fallout fuel-air ratio calculated from the above relation. The exhaust stroke then returns the charge to the original volume, and with isentropic expansion is assumed, one obtains

$$\rho_4 = (1 + f)\rho_1 \tag{6}$$

$$\frac{p_4}{p_3} = \left(\frac{\rho_4}{\rho_3}\right)^{\gamma} \tag{7}$$

and expansion temperature is calculated from the ideal gas law. Turbocharger exhaust conditions were then simply

$$T_5 = T_4 - \frac{Spa_{turbocharger}}{cp} \tag{8}$$

With the gas conditions defined for all parts of the cycle, the indicated fuel conversion efficiency, $\eta_{f,i}$ as well as indicated mean effective pressure, imep (the work per cycle per chamber volume) can be determined.

$$\eta_{f,i} = \frac{W_{c,i}}{m_f * Q_{LHV}} = \frac{(h_4 - h_3) - (u_2 - u_1) + \frac{p_4}{\rho_4} - \frac{p_2}{\rho_2}}{f Q_{lhv}} = 1 - \frac{T_4 - T_1}{\gamma(T_3 - T_2)} \tag{9}$$

$$imep = \frac{W_{c,i}}{V_d} = f Q_{lhv} \rho_1 \frac{r_c}{r_c - 1} \eta_{f,i} \tag{10}$$

With the indicated mean effective pressure defined, the power available compared to the sea level static conditions can be estimated as

$$\frac{P_a}{P_0} = \frac{imep}{imep_0} \tag{11}$$

assuming that engine operating speed is not a strong function of ambient conditions. Note that turbocharged engines normally limit their power output via a wastegate which diverts airflow away from the turbocharger (to prevent overpressurization of the engine), and thereby reduce the $Spa_{turbocharger}$ term. To simulate wastegate operation, $Spa_{turbocharger}$ was determined based on the power required to make $P_a/P_0=1$ below the break altitude for the standard atmosphere (taken from engine data), and held constant above this altitude, i.e.

$$Spa_{turbocharger} \leq Spa_{turbocharger,break} \tag{12}$$

To illustrate, $Spa_{turboacharger}$ for both standard as well as "hot" atmospheres (defined here as $T_{hot}=T_{std}+20K$) is plotted below, with $Spa_{turboacharger,break}$ corresponding to a "break" altitude of 6000 ft. for standard atmospheric conditions.

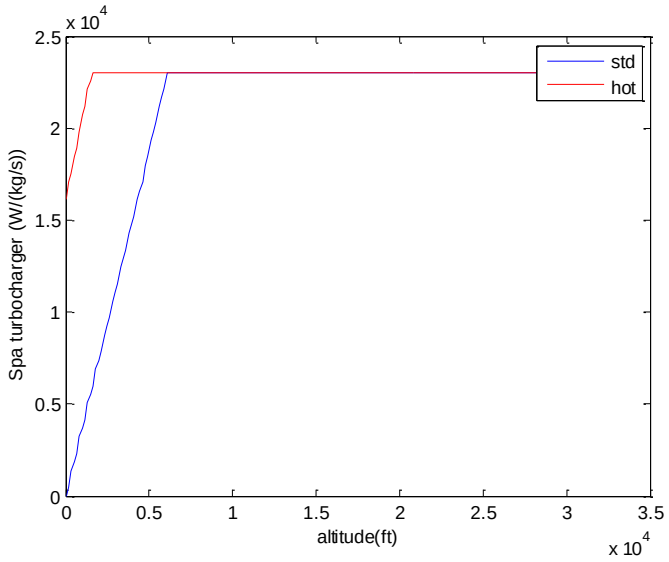

Figure 1: Cycle Analysis Turbocharger Specific Power

To estimate the accuracy of the turbocharger model, a centrifugal compressor map is scaled based on the pressure ratio and corrected mass flow ratio at the breakpoint. The original map is repeated below, with a reference corrected mass flow of .205 kg/s and pressure ratio of 2.05.

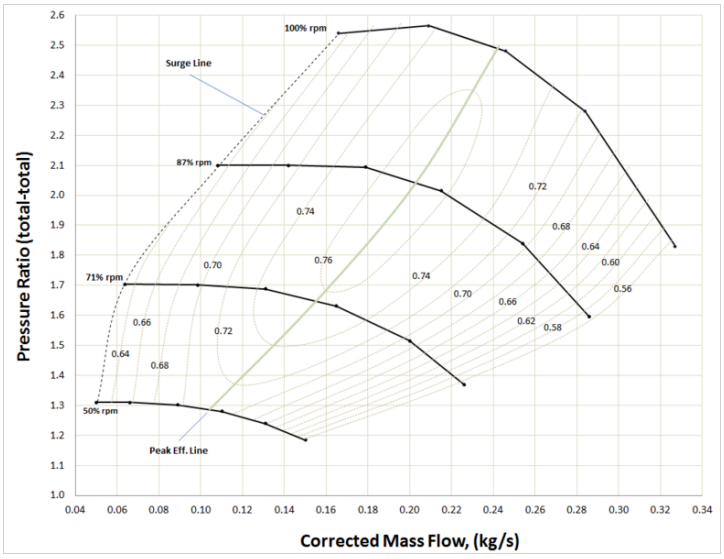

Figure 2: Centrifugal Compressor Map

The surge line was defined based on the break pressure ratio of the turbocharger, and is plotted in Figure 3 vs. the corrected mass flow normalized by the break point mass flow, along with the pressure ratio for standard and "hot" atmospheres.

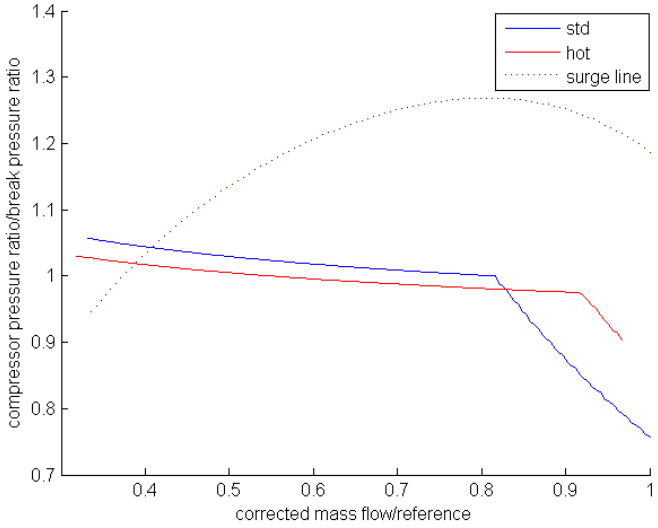

Figure 3: Compressor Surge

For constant power output, both the standard as well as hot atmosphere engine cycles appear to fall below the surge line for the bulk of the altitude range shown here. Note that publically available data on the Centurion 2.0s only extend to an altitude of 24,000 ft., or a corrected mass flow ratio of ~.42, which is slightly beyond the crossover point of about .4. Similarly, the turbine pressure ratio was plotted versus corrected mass flow for the two atmospheric conditions.

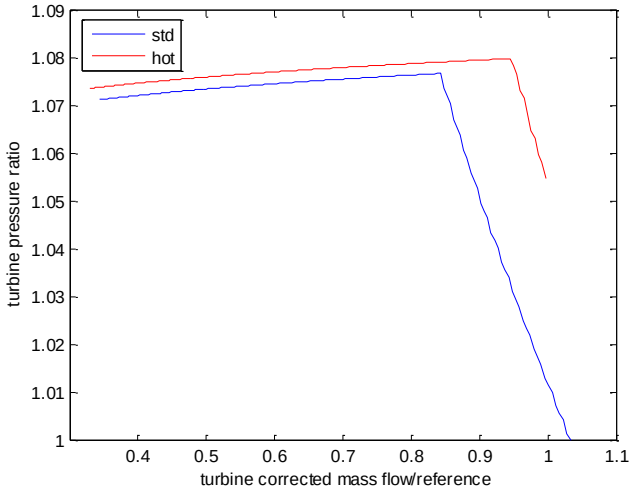

Figure 4: Turbine Pressure Comparison

The turbine pressure ratio for the standard atmosphere falls below the hot atmospheric conditions in the figure above, indicating that the assumptions here may be somewhat optimistic for "hot" temperature conditions; however there is only about a ~2-4% difference between the curves at any of the given operating points; thus, other assumptions, such as a perfect gas, as well as isentropic compression and expansion may be more significant.

DIESEL ENGINE MODELING

Substituting in standard sealevel atmospheric values for γ, cp, and R, along with normal operating parameters for T_3 and rc into the cycle analysis Pa/P_0 term results in a complex function based on the freestream temperature ratio (θ) as well as the $Spa_{turbocharger}$ term, but is only linear with the freestream pressure ratio (δ). To that end, the engine was assumed to lapse linearly with a proposed lapsing parameter $Y=\delta * \theta^{x_t}$, where the x_t term varies from engine to engine. The cycle analysis was then queried for a variety of $Spa_{turbocharger}$ values, along with a range of θ, with a power law used to determine the "best fit" for the coefficient x_t. A plot of this is shown in Figure 5 below, with no limit on Pa/P_0 (i.e. the wastegate is fully closed for the range of operation). Figure 6 shows the results of plotting a temperature sweep of the cycle analysis model vs. the "best fit" Y for a given turbocharger specific power.

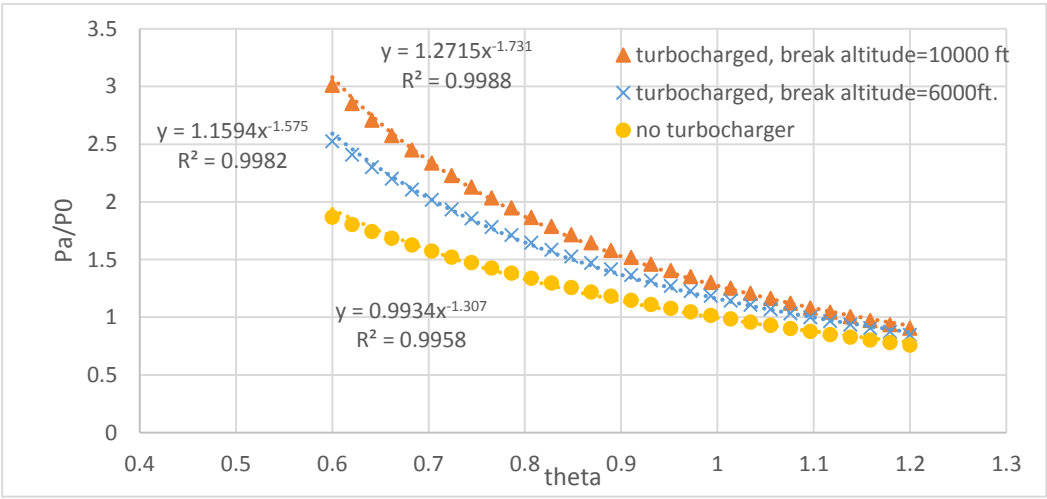

Figure 5: Cycle Analysis Temperature Sweep

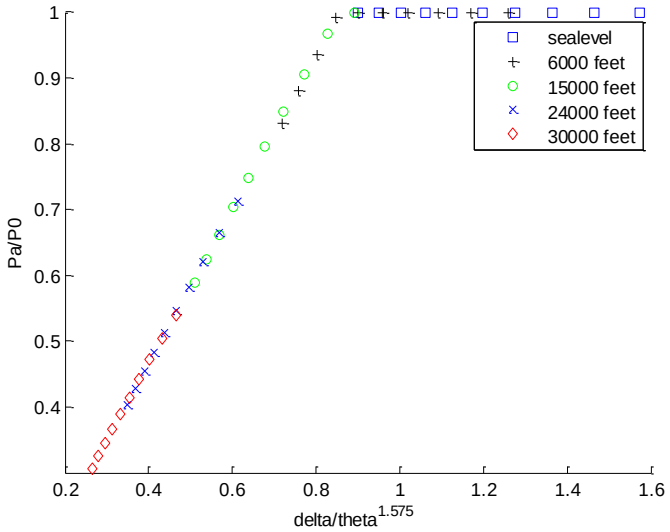

Figure 6: Cycle Analysis Temperature Sweep (break altitude=6000 ft.)

Figure 6 illustrates that, under these assumptions, the parameter Y causes the 0D model to collapse to a line. To that end, a proposed turbocharged diesel engine model for conceptual design that takes into account a variety of atmospheric conditions as well as varying engine speeds can be seen below.

$$Y=\delta * \theta^{x_t} \tag{13}$$

$$\frac{P_a}{P_0} = \frac{P_{ref}}{P_0}\left(\frac{N}{N_{spec}}\right) \; if\, Y \geq Y_{break}\left(\frac{N}{N_{spec}}\right) \; or \frac{P_a}{P_0} > \frac{P_{ref}}{P_0}\left(\frac{N}{N_{spec}}\right) \tag{14}$$

$$\frac{P_a}{P_0} = Ks_1\left(\frac{N}{N_{spec}}\right) * Y + Ks_0\left(\frac{N}{N_{spec}}\right) \; if\, Y < Y_{break}\left(\frac{N}{N_{spec}}\right) \tag{15}$$

$$K_{s1}\left(\frac{N}{N_{spec}}\right) = Ks_{11} * \frac{N}{N_{spec}} + Ks_{10} \tag{16}$$

$$K_{s0}\left(\frac{N}{N_{spec}}\right) = Ks_{01} * \frac{N}{N_{spec}} + Ks_{00} \tag{17}$$

$$\frac{P_{ref}}{P_0}\left(\frac{N}{N_{spec}}\right) = Kr_{01} * \frac{N}{N_{spec}} + Kr_{00} \tag{18}$$

$$Y_{break}\left(\frac{N}{N_{spec}}\right) = Ksi_{01} * \frac{N}{N_{spec}} + Ksi_{00} \tag{19}$$

Where x_t, Ks_{11}, Ks_{10}, Ks_{01}, Ks_{00}, Kr_{01}, Kr_{00}, Ksi_{01}, Ksi_{00} are inputs to the model, calibrated to fit a particular engine. Note that P_{ref}/P_0 (N/N_{spec}) refers to P_{ref}/P_0 as a function of N/N_{spec}. This model simulates turbocharging up to the breakpoint and tends to fit the data very well for the standard atmosphere as seen below, which compares data taken from the Centurion 2.0s engine with fits to this model.

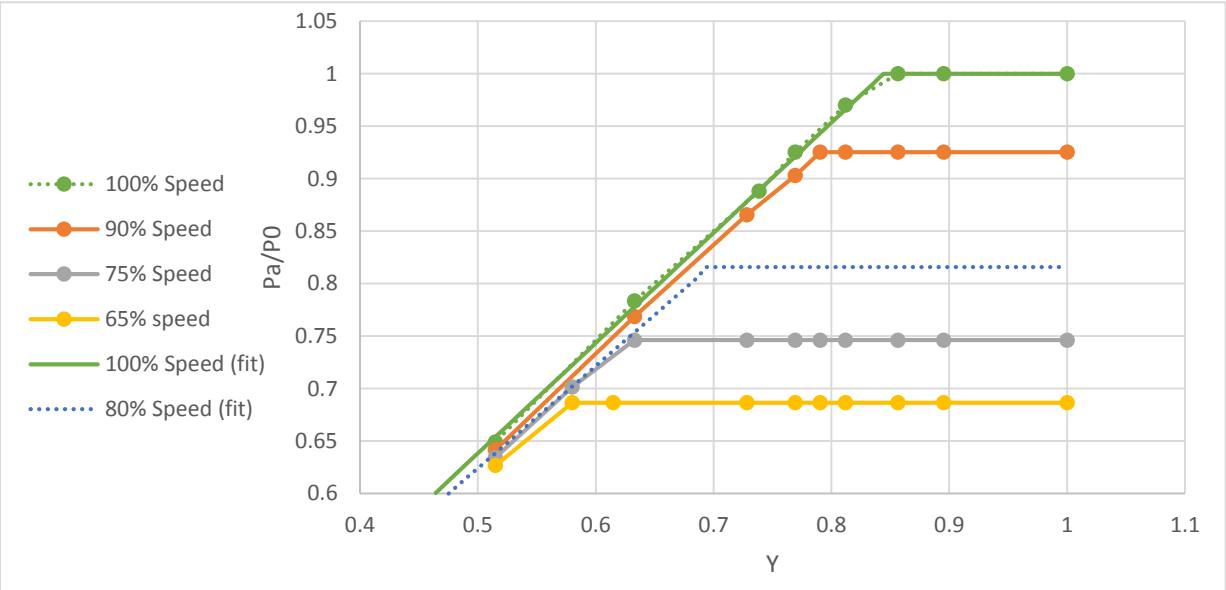

Figure 7: Centurion 2.0s Model

Figure 8 shows the lapsing of the linear-fit model of the Centurions 2.0s engine (assuming 100% engine speed) based on the parameter Y, a comparable 0D cycle analysis of the engine, along with raw data.

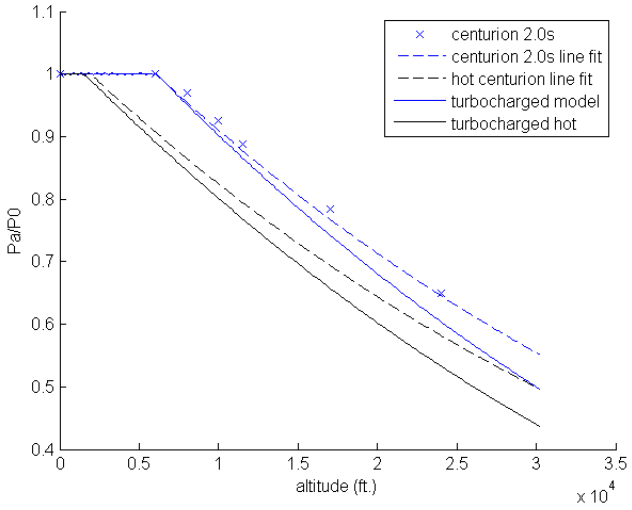

Figure 8: Comparison of Cycle Analysis and Linear Model

As can be seen in Figure 8, the impact of changing atmospheric conditions between the linear and 0D cycle analysis is qualitatively quite similar. Both the linear model and the 0D-cycle break at approximately the same altitude, and follow roughly the same trend in standard and "hot" atmospheric conditions; notably, the performance difference between standard and "hot" atmospheres is comparable. However, turbocharged engines are somewhat complicated, and critical altitude is largely a function of wastegate operation. The cycle analysis subsumes wastegate operation into the $Spa_{turbocharger}$ term. Furthermore, the cycle analysis model does not take into account other aspects of engine operation, or other processes that may be used, such as intercooling. Figure 9 shows how the parameter fit model from equations (13)-(19) compares to three different turbocharged diesel engines.

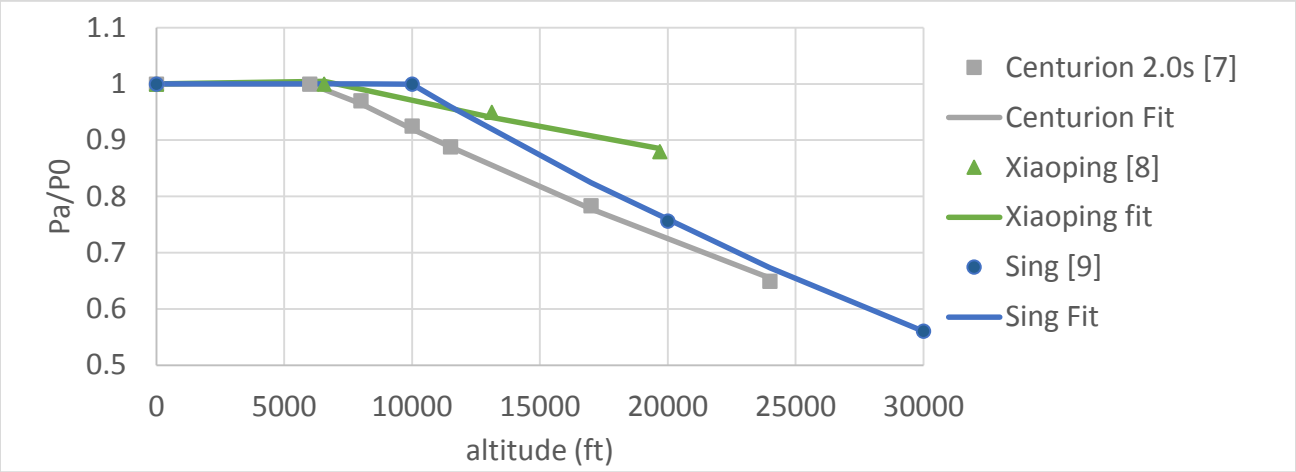

Figure 9: Diesel Engine Lapse (Standard Atmosphere)

As Figure 9 shows, the model is able to approximate the data to reasonable accuracy for a variety of different diesel engines. However, for hot and high conditions, there is still a large degree of uncertainty in the simple parameter fit model, which fits the data well for standard atmospheres, but unfortunately, data is sparse for other atmospheric conditions; the cycle analysis allows some basis to estimate performance according to this parameter, but higher fidelity analysis is nonetheless recommended. Figure 10 below compares the parameter fit model for the Centurion 2.0s for both standard and hot conditions to a representative turboshaft model illustrating their differing lapsing characteristics [10].

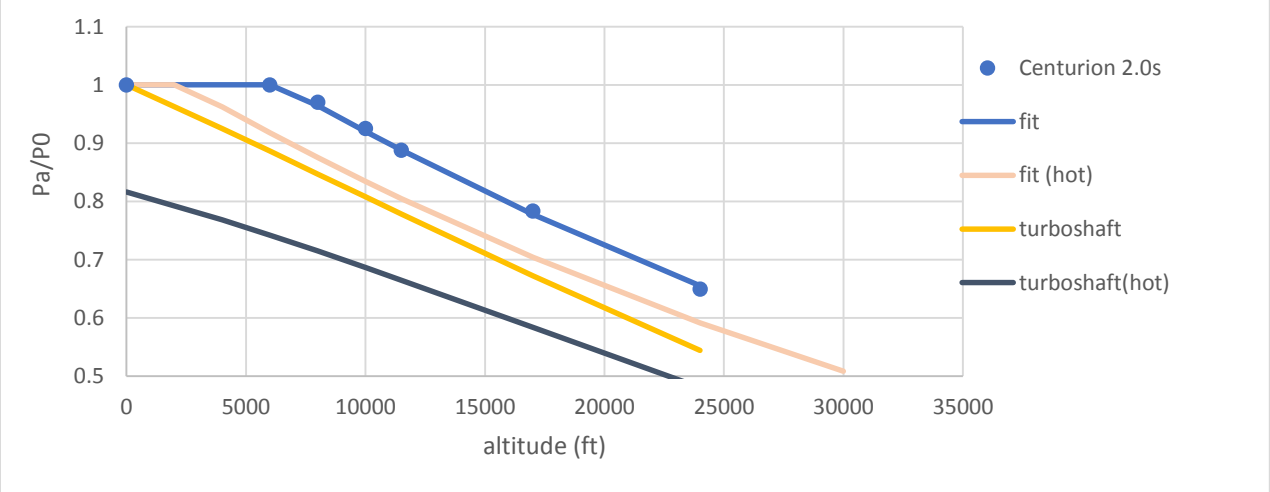

Figure 10: Model Comparison for Nonstandard Atmospheres

THROTTLE AND WEIGHTS

A simple cubic fit for fuel flow vs. the ratio of power required to power available has been proposed and is shown below. A fit for a representative diesel engine is shown in Figure 11 [11].

$$\dot{w} = \dot{w}_0 * (Kffp_0 + Kffp_1 * (\frac{P}{P_a}) + Kffp_2 * \left(\frac{P}{P_a}\right)^2 + Kffp_3 * \left(\frac{P}{P_a}\right)^3) \quad (20)$$

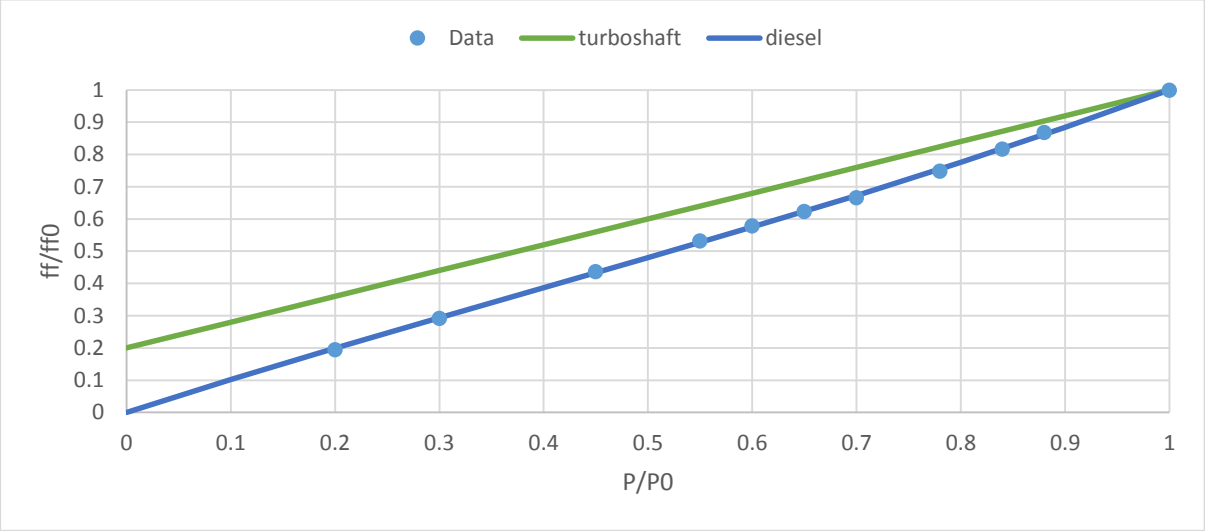

Figure 11: Fuel Flow vs. Power

Note that the diesel engine appears to operate more efficiently than the turboshaft engine in the off-design condition, as one might expect; diesel engines are known to run at relatively high efficiencies, even at lower power outputs [4]. Knowing that diesel engines suffer from low power-to-weight ratios, obtaining a reasonable weights correlation is critical in evaluating their use in conceptual design. To that end, data from a wide range of diesel engines of varying power capabilities were collected, and a scaling law was formed to fit the data. A scaling correlation was also developed for high power-to-weight electric motors. These were then compared with an equivalent scaling law for turboshaft engines shown in Figure 12 below.

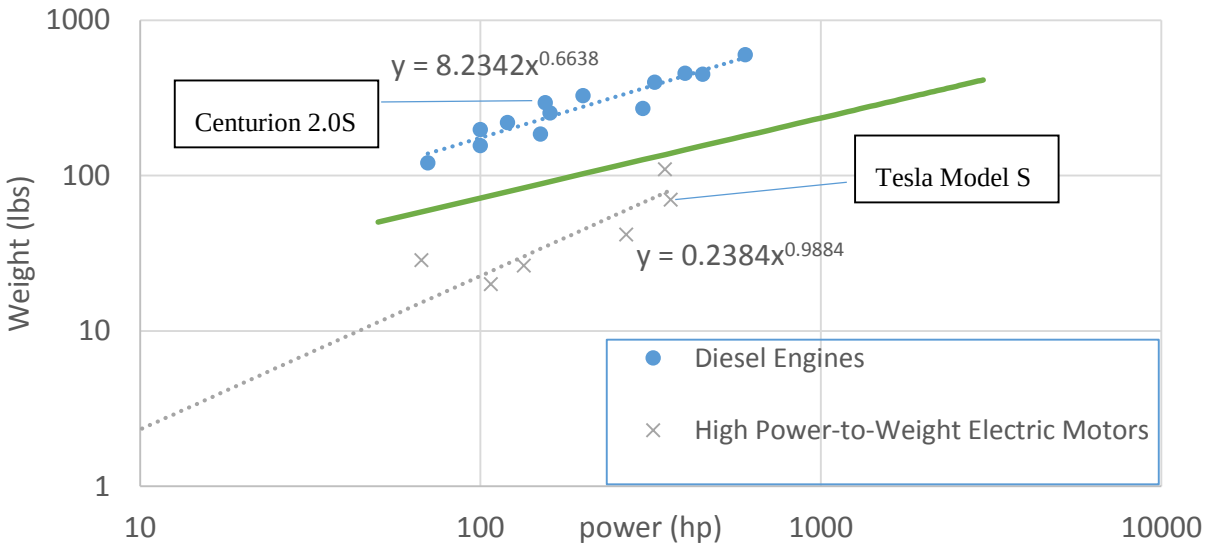

Figure 12: Diesel Weight Scaling

Figure 12 demonstrates that, for comparable power output, both turboshaft engines and state of the art electric motors tend to offer far superior power-to-weight ratios over diesel engines. However, when including the required energy systems (such as batteries), this may not necessarily be the case. Note that electric systems are relatively scale invariant (i.e. their power-to-weight ratio does not change substantially with size). Thus, the motor exponential coefficient of .9884 should not be terribly surprising.

DESIGN APPROACH

As a baseline, an unmanned tailsitter designed to carry a 200 lb. payload was designed and sized using a turboshaft engine; the mission is as follows: 2 minute hover at 6000 ft. and 95°F (6K95), climb to a specified cruise altitude, cruise 232 nautical miles, descend to 6000 ft., hover for 30 minutes, climb back to cruise altitude, cruise and descend 232 miles, hover for 1 minute at 6000 ft., and fly for 10 minutes at cruise speed as a reserve segment. A diagram of flight speed, altitude, and horsepower vs time can be seen below in Figure 13, along with some reference parameters in Table 2. A CAD drawing of the aircraft can be seen in Figure 14.

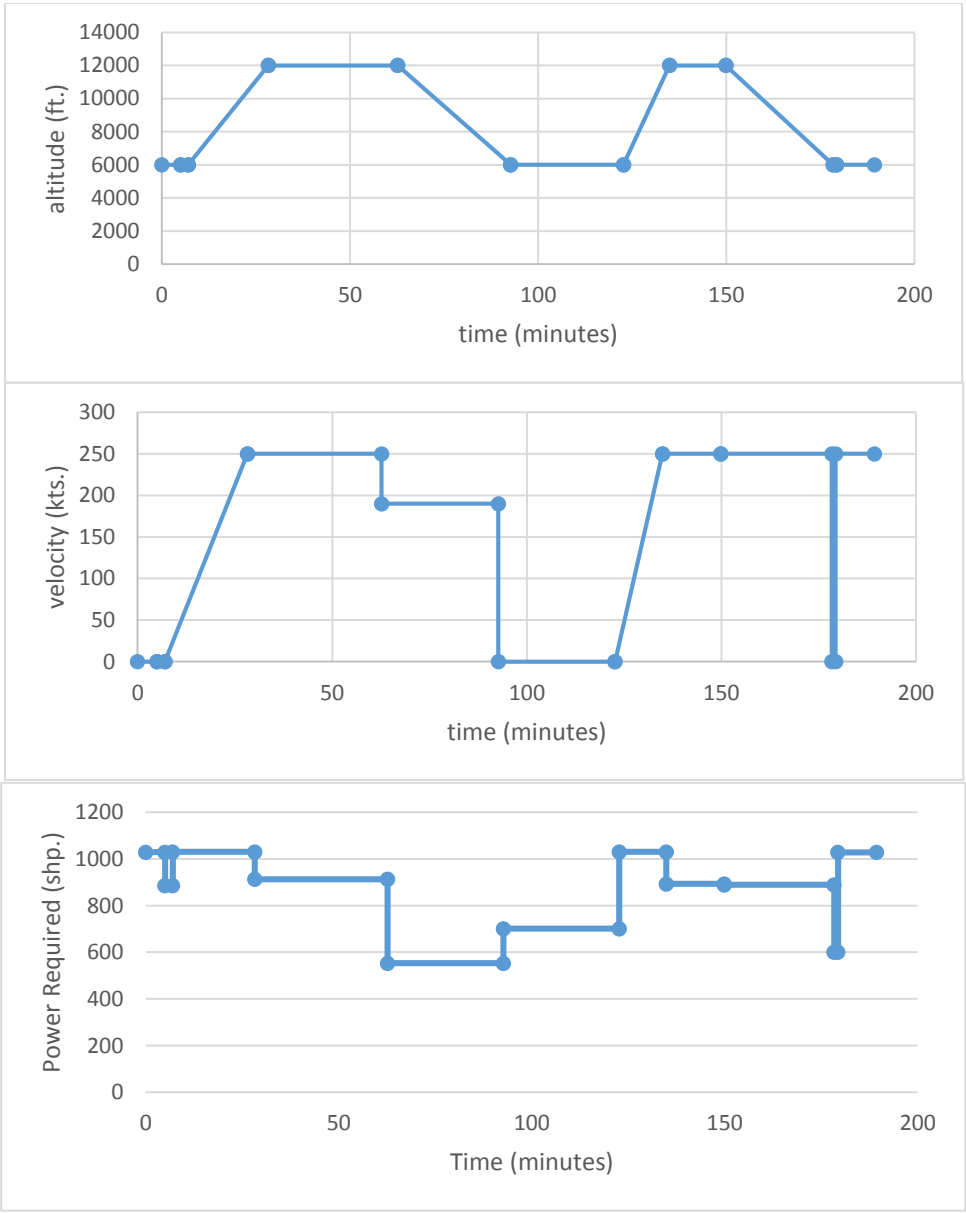

Figure 13: Baseline Turboshaft Mission

Table 1: Reference Aircraft

DGW (lbs.)	Mission Fuel (lbs.)	Engine Power (hp)	Disk Loading (psf.)	Wing Loading (psf.)	Climb Velocity (kts.)	Cruise Velocity (kts.)	Loiter Velocity (kts.)	Rotor Tip Speed (Hover, kts.)	Rotor Tip Speed (Hover, kts.)	Design Altitude (ft.)
5443.3	1450.5	812.0	8	60	250	250	190	700	700	12,000

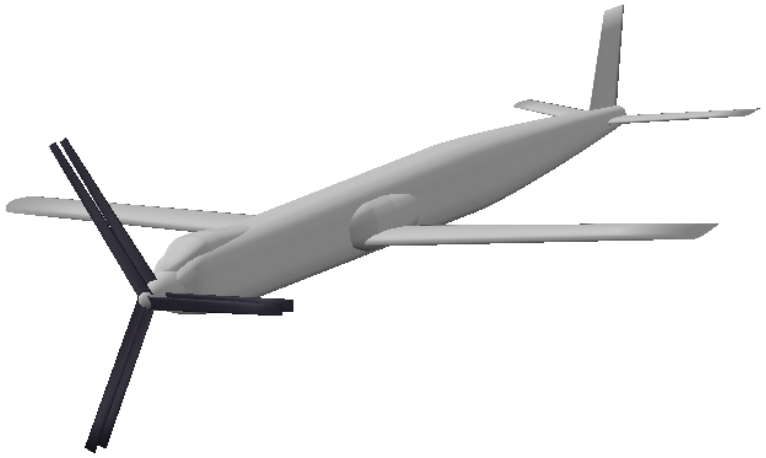

Figure 14: Reference Aircraft

With the reference design capabilities sized and established, three different categories of aircraft were developed and optimized using a combination of NDARC and OpenMDAO. NDARC is a conceptual design environment capable of modeling a variety of aircraft, including tiltrotors, tailsitters, as well as helicopters [12]. NDARC uses simplified physical representations, semi-parametric, and parametric models to represent the aircraft. Recent work has extended NDARC's architecture to include models necessary to design electric and hybrid aircraft [10]. OpenMDAO is a python-based architecture which allows for communication between different analysis codes with the goal of creating a framework for optimization [13].

Diesel-powered aircraft were first sized using the same disk loading, wing loading, and mission profile as the reference aircraft. Two of the major differences between diesel and turboshaft engines are the different lapsing behavior (as shown in Figure 10) and throttling behavior (Figure 11), in addition to power-to-weight ratio. To that end, design sweeps of diesel aircraft vs. design altitude and cruise velocity were made, with the resulting fuel requirements and fuel weight fractions shown in Figures 15 and 16.

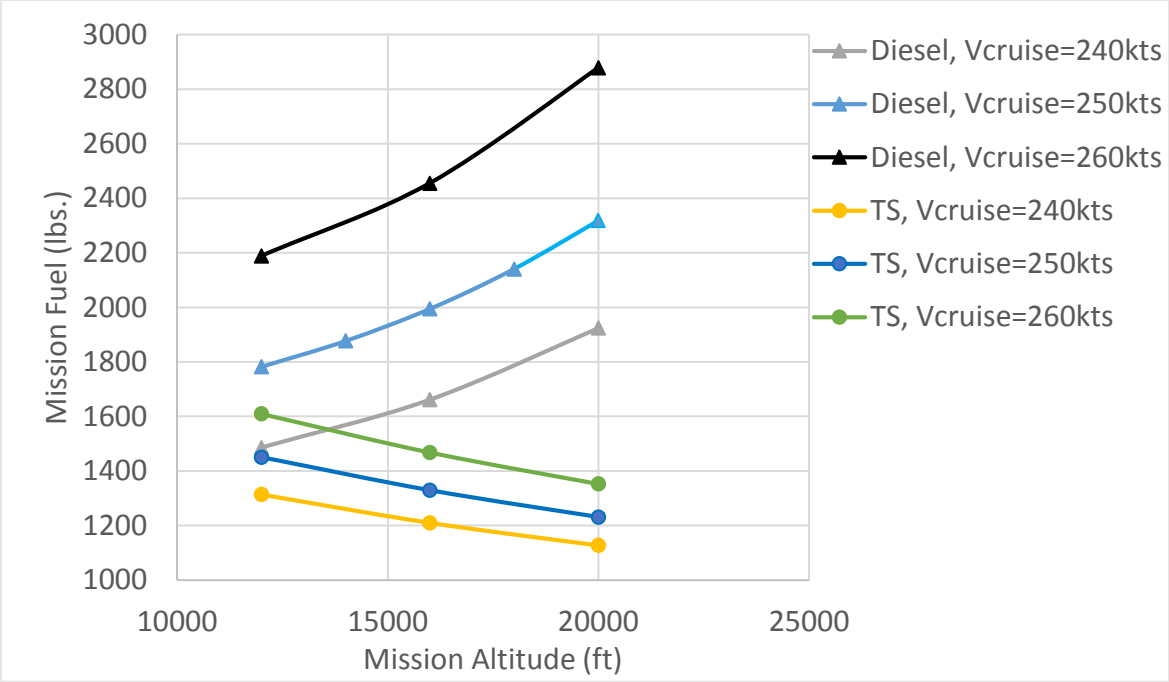

Figure 15: Mission Fuel Design Sweep

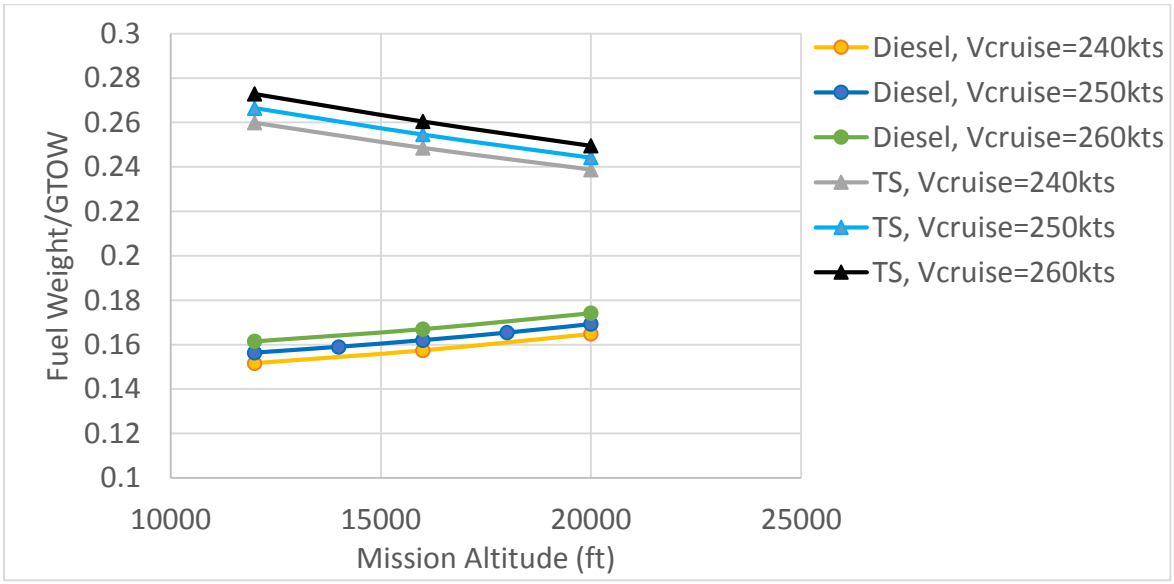

Figure 16: Fuel Fraction Design Sweeps

For the reference mission and design, the turboshaft burns less fuel compared to the all-diesel aircraft. Furthermore, both aircraft burn less fuel when designed to fly at a lower cruise velocity. However, the diesel engine aircraft prefer to fly at lower altitudes; the diesel aircraft here are power-limited at cruise, unlike the turboshaft aircraft. Thus, reducing the cruise altitude appears to decrease the GTOW of the vehicle as it significantly lowers the required engine size. The engines on the turboshaft aircraft, on the other hand, are significantly more efficient at higher altitudes, which more than offsets the weight penalty from increasing the engine size. In addition, the fuel weight fraction of the diesel aircraft is much lower, due to the superior specific fuel consumption of diesel engines over turboshafts; the extra fuel requirements come as a result of a larger aircraft due to the poor power-to-weight ratio of

diesel engines. For reference, the turboshaft aircraft possessed a much lower gross takeoff weight (~5,000 lbs.) compared to the diesel (~11,000 lbs.).

To reduce the overall size of the diesel engine a parallel hybrid diesel-electric propulsion scheme has been devised. The battery and motor were sized to meet an additional power demand for hover for two minutes at the 6K95 condition for a given input motor power, while the diesel engine provides whatever additional power demands the mission requires, flying the rest of the mission as an all-diesel aircraft. Figure 17 displays a sweep of GTOW and mission fuel requirement vs. motor power at the reference aircraft conditions.

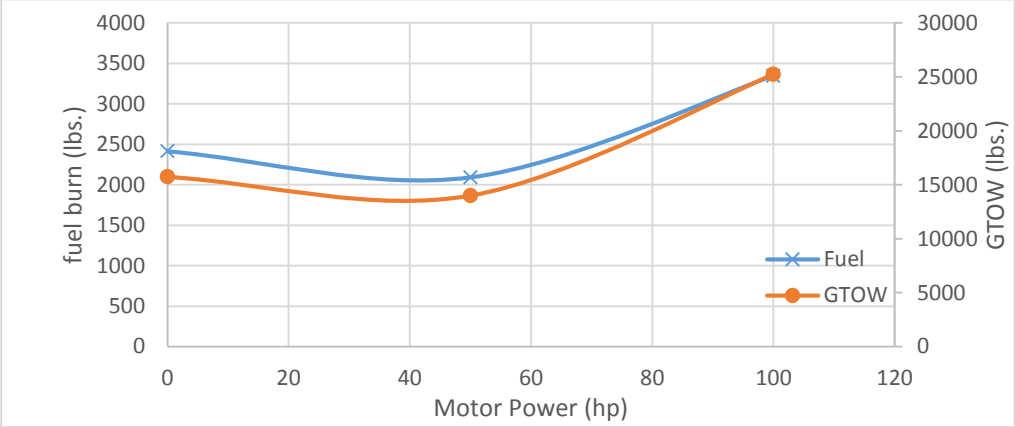

Figure 17: Motor Power Design Sweep

Figure 17 indicates that including electrics in this system may result in reductions in GTOW as well as fuel burn, as it helps ameliorate some of the weight penalties coming from the poor specific power of diesel engines. Additionally, the decreased fuel requirements for the hybrid system primarily come as a result of cascading weight reductions due to the reduced propulsion system weight; to compare, for a motor power of 50 hp., there is a 3.9% lower GTOW and 3.8% lower fuel burn when compared to the reference all-diesel aircraft. When plotting these results as a function of electric system power normalized by the diesel engine power, an interesting result emerges, as seen below.

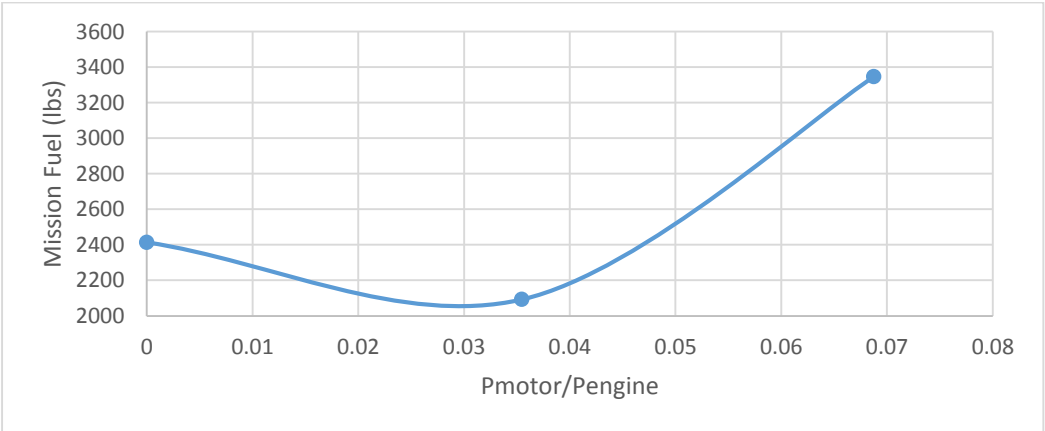

Figure 18: Mission Fuel vs. Electric Power Fraction

Figure 18 indicates that, for the reference design and mission, reduction in aircraft size and fuel burn may occur when only a small percentage of the overall power requirements come from the motor/battery. However, from the baseline design parameters, these benefits only appears in a very narrow range of power ratios. This may result in difficulties in optimizing the aircraft and evaluating a broader region of the design space, as it may be indicative of a preponderance of local minima.

With this in mind, three different classes of aircraft were optimized to these requirements: a turboshaft-powered aircraft, a purely diesel-powered aircraft, and a diesel-electric hybrid aircraft. The objective function for the given mission was fuel burn, with constraints to ensure feasibility in the mission, that the propulsion system meets all power and energy requirements, and that the aircraft meets all trim conditions. Design variables were gross takeoff weight (GTOW), disk loading, wing loading, fuel capacity, engine power (diesel or turboshaft), rotor tip speed in hover as well as fraction tip speed in cruise, climb velocity, cruise velocity, loiter velocity, along with the design altitude. Furthermore, for the electric case, the motor power normalized by the engine power along with the battery energy were also used. The optimizer of choice was a PyOpt OpenMDAO plugin of NSGA2, a genetic-algorithm, chosen both for a global sweep of the design space, as well as its ability to ignore unfeasible cases (such as NaNs in NDARC outputs) [14,15]. Table 3 summarizes the final designs.

Table 2: Optimized Aircraft Comparison

	Turboshaft	Diesel	Diesel-Electric	Lower Bound	Upper Bound
GTOW (lbs.)	4087	8,838	8,077	2000	25,000
Disk Loading (psf.)	8.00	8.46	8.00	8	25
Wing Loading (psf.)	55.0	55.0	55.0	55	140
Fuel Tank Capacity (lbs)	1392	2157	1,633	50	7,000
Engine Power (hp.)	502.1	930	707	200	5,000
Rotor Tip Speed (ft/s)	800	748	681	500	850
Fraction Tip Speed Cruise	.795	.852	.424	.4	.99
t/c	.150	.158	.154	.15	.3
Climb Velocity (kts.)	163	150	154	50	250
Cruise Velocity (kts.)	200	152	165	50	300
Loiter Velocity (kts.)	166	128	140	50	300
Design Altitude (ft.)	28,000	10,000	10,000	10,000	28,000

Motor Power/Engine Power	N/A	N/A	.16	.01	.3
Battery Energy (MJ)	N/A	N/A	3.6	.1	10
Mission Fuel (lbs.)	790.1	1028.9	1003.9		

From Table 3, all three designs were driven to low disk loadings and wing loadings. The turboshaft design however tended towards higher design altitudes and cruise velocities, while the diesel aircraft possessed lower design altitudes and velocities. This is due to tradeoffs between power requirements and engine efficiency, which were shown in Figures 15 and 16. The diesel-electric aircraft here possessed only slightly lower fuel burn over the pure diesel aircraft, albeit with substantial weight savings, with a significantly lower rotor speed at cruise. Nonetheless, for the mission requirements and assumptions here, the turboshaft design outperforms both the diesel as well as diesel electric designs in GTOW and fuel burn. However, there may be design requirements and frameworks in which the diesel or diesel-electric aircraft can outperform an equivalent turboshaft design, and improving battery technology is likely to help close the gap. On the other hand, satisfying power and energy consistency requirements proved difficult for the optimizer, and there may be designs not featured here that exhibit greater fuel burn benefits. Further study is recommended, both of aircraft configurations as well as formulations of the problem to determine any additional improvements.

CONCLUSIONS

Diesel engine models have been developed for the conceptual design of both diesel and diesel-electric rotorcraft based on a combination of 0D thermodynamic models and fits to published data. Results were then extrapolated to a tailsitter design, with design sweeps and optimization studies used to evaluate design tradeoffs. For the mission and vehicle architecture here, the turboshaft design appears to outperform comparable diesel and diesel-electric aircraft. Additionally, the diesel aircraft "prefer" to fly at lower operating altitudes (to reduce engine weight penalties). Small improvements in weight as well as fuel burn can be found in the diesel-electric aircraft in comparison to the diesel. However, results indicated numerical difficulties in the optimization process. As a result, further study of alternative aircraft configurations and problem formulations is recommended.

AKNOWLEDGEMENTS

Michael Vegh would like to acknowledge the support of thee Science, Mathematics and Research for Transformation (SMART) Scholarship for Service Program. The authors would also like to acknowledge Wayne Johnson for his assistance in making the necessary modifications to NDARC to produce the results shown here.

REFERENCES

[1] Vegh, J.M., Alonso, J., Orra, T.,Ilario da Silva, C., "Flight Path and Wing Optimization of Lithium-Air Battery Powered Passenger Aircraft," AIAA 2015-1674 53rd AIAA Aerospace Sciences Meeting, AIAA SciTech, Kissimmee, FL, January, 2015.

[2] Moore, M. and Fredericks, B., "Misconceptions of Electric Propulsion Aircraft and their Emergent Aviation Markets," AIAA SciTech, NASA Langley Research Center, National Harbor, Maryland, 2014.

[3] Hepperle, M., "Electric Flight- Potential and Limitations," German Aerospace Center, 2012.

[4] Daidzic, N., Piancastelli, L., and Cattini, A., "Diesel Engines for Light-to-Medium Helicopters and Airplanes (Editorial)," International Journal of Aviation, Aeronautics, and Aerospace, Vol. 1, Issue 3, Article 2, August 2014.

[5] Fredericks, W., Moore, M., and Busan, R., "Benefits of Hybrid-Electric Propulsion to Achieve 4x Increase in Cruise Efficiency for a VTOL Aircraft," NASA Langley Research Center, Hampton, VA.

[6] Heywood, J., *Internal Combustion Engine Fundamentals*, McGraw-Hill, New York, NY, 1988.

[7] "Aircraft Engine," Centurion 2.0s Specs, Continental Motors, Warrendale, July 2015, [http://continentaldiesel.com/typo3/fileadmin/_centurion/pdf/Datenblaetter/DS_CMG_1_CD-135.pdf. Accessed 8/25/2015]

[8] Xiaoping, B., Zhang, G., and Zheng, Xiaojing, "Predicting Turbocharged Diesel Engine Performance at Altitude," Chinese Armed Forces Center, Society of Automotive Engineers, 1996.

[9] Sing, Shaitan, "VRDE Developing Aero-Diesel Engine for UAVs," Indian Defence Forum, May 2015, [http://defence.pk/threads/vrde-developing-aero-diesel-engine-for-uavs.375587/. Accessed 8/25/2015]

[10] Johnson, W., "Propulsion System Models for Rotorcraft Conceptual Design," 5th Decennial AHS Aeromechanics Specialists Conference, San Francisco, CA, 2014.

[11] Heywood, J., and Sher, E., *The Two-Stroke Cycle Engine: Its Development Operation, and Design*, Society of Automotive Engineers, Warrendale, PA, 1999.

[12] Johnson, W., "NDARC: NASA Design and Analysis of Rotorcraft," NASA/TP-2009-215402, Moffett Field, CA, 2009.

[13] Gray, J. S., Moore, K. T., and Naylor, B. A., "OPENMDAO: An Open Source Framework for Multidisciplinary Analysis and Optimization," 13th AIAA/ISSMO Multidisciplinary Analysis and Optimization Conference, Fort Worth, TX, AIAA, AIAA-2010-9101, AIAA, Fort Worth, Texas, August 2010.

[14] Perez R.E., Jansen P.W., and Martins J.R.R.A. (2012) "pyOpt: A Python-Based Object-Oriented Framework for Nonlinear Constrained Optimization, Structures and Multidisciplinary Optimization," 45(1):101-118.

[15] Deb K., Pratap A,. Agarwal .S, Meyarivan T., "A Fast and Elitist Multiobjective Genetic Algorithm: NSGA-II." Evolutionary Computation, IEEE Transactions on 6(2):181–197, (2002)